Bright triplet excitons for efficient X-ray excited luminescence

Xiao Wang
Northwestern Polytechnical University
Huifang Shi
Key Laboratory of Flexible Electronics & Institute of Advanced Materials, Nanjing Tech University
https://orcid.org/0000-0002-0172-3230
Huili Ma
Key Laboratory of Flexible Electronics & Institute of Advanced Materials, Nanjing Tech University
Wenpeng Ye
Nanjing Tech University (NanjingTech)
Lulu Song
Nanjing Tech University (NanjingTech)
Jie Zan
Fuzhou University
Xiaokang Yao
Nanjing Tech University (NanjingTech)
Xiangyu Ou
Fuzhou University
Guohui Yang
Nanjing Tech University (NanjingTech)
Zhu Zhao
Nanjing Tech University (NanjingTech)
Manjeet Singh
Nanjing Tech University (NanjingTech)
Chongyang Lin
Nanjing Tech University (NanjingTech)
He Wang
Key Laboratory of Flexible Electronics & Institute of Advanced Materials, Nanjing Tech University
Wenyong Jia
Nanjing Tech University (NanjingTech)
Qian Wang
Nanjing Tech University (NanjingTech)
Jiahuan Zhi
Nanjing Tech University (NanjingTech)

Chaomin Dong
Nanjing Tech University (NanjingTech)
Xueyan Jiang
Nanjing Tech University (NanjingTech)
Yongan Tang
Shenzhen University
Xiaoji Xie
Nanjing University of Technology https://orcid.org/0000-0002-4830-1246
Yang Yang
Zhejiang University https://orcid.org/0000-0002-3362-7155
Jianpu Wang
Nanjing Tech University https://orcid.org/0000-0002-2158-8689
Qiushui Chen
Fuzhou University
Yu Wang
National University of Singapore
Huang-Hao Yang
Fuzhou University
Guoqing Zhang
Hefei National Laboratory for Physical Sciences at the Microscale, University of Science and Technology of China
Zhongfu An
Key Laboratory of Flexible Electronics & Institute of Advanced Materials, Nanjing Tech University https://orcid.org/0000-0002-6522-2654
Xiaogang Liu
National University of Singapore https://orcid.org/0000-0003-2517-5790
Wei Huang (iamdirector@fudan.edu.cn)
Northwestern Polytechnical University https://orcid.org/0000-0001-7004-6408

Research Article

Keywords: X-ray excited luminescence, triplet excitons, organic phosphors

Posted Date: August 31st, 2020

DOI: https://doi.org/10.21203/rs.3.rs-57892/v1

Version of Record: A version of this preprint was published at Nature Photonics on January 11th, 2021.
See the published version at https://doi.org/10.1038/s41566-020-00744-0.

Bright triplet excitons for efficient X-ray excited luminescence

Xiao Wang[1,8], Huifang Shi[2,8], Huili Ma[2], Wenpeng Ye[2], Lulu Song[2], Jie Zan[3], Xiaokang Yao[2], Xiangyu Ou[3], Guohui Yang[2], Zhu Zhao[2], Manjeet Singh[2], Chongyang Lin[2], He Wang[2], Wenyong Jia[2], Qian Wang[2], Jiahuan Zhi[2], Chaomin Dong[2], Xueyan Jiang[2], Yongan Tang[4], Xiaoji Xie[2], Yang (Michael) Yang[5], Jianpu Wang[2], Qiushui Chen[3], Yu Wang[4], Huanghao Yang[3], Guoqing Zhang[6], Zhongfu An[1,2*], Xiaogang Liu[7*] and Wei Huang[1,2*]

Materials that exhibit X-ray excited luminescence have great potential in radiation detection, security inspection, biomedical applications, and X-ray astronomy[1-4]. However, such materials are almost exclusively limited to inorganic crystals, which are typically prepared under high temperatures[5]. Herein, we report a design principle of purely organic phosphors to boost X-ray excited luminescence with sufficient utilization of triplet excitons. Our experimental data reveal that proportion of emission from bright triplet excitons is significantly improved upon X-ray irradiation, compared with UV excitation. These organic phosphors have a detection limit of 33 nGy/s, which is 167 times lower than the standard dosage for X-ray medical examinations. We further demonstrated their potential application in X-ray radiography, which can be conveniently recorded using a digital camera. These findings illustrate a fundamental principle to design efficient X-ray excited purely organic phosphors, propelling the development of radioluminescence related applications.

X-ray-responsive materials generally display large X-ray attenuation coefficients because of high atomic number elements, which have aroused intense research interest owing to their wide applications in bioimaging, radiotherapy, and non-destructive defect detection of industrial products[6-10]. Such X-ray-responsive materials include non-emissive radiocontrast agents (e.g., iohexol and iopromide) and scintillators that can convert high energy X-ray beam into low-energy visible photons[2,11,12]. To date, almost all reported X-ray-sensitive materials are limited to inorganic phosphors or organometallic materials containing heavy metals[13]. Purely organic materials, also termed as metal-free organic phosphors, have congenital advantages as scintillator candidates, including abundant resources, flexibility, mild preparation conditions, and environmental friendliness. However, weak X-ray absorption and low exciton utilization hinder the development of purely organic scintillators[12], leaving it a formidable challenge. Purely organic phosphors are mainly made up of light atoms, such as C, H, N, *etc*., resulting in weak absorbance of X-ray (attenuation coefficient $\mu \propto Z^4$, Equation S1). Besides, there only exists fluorescence from singlet excitons upon irradiation owing to weak spin-orbit coupling (SOC). In principle, almost all triplet excitons, accounting for about 75%, are wasted, which is attributed to the 'dark state' feature of the triplet excitons in traditional purely organic phosphors.[14-16]

Recently, phosphorescence from bright triplet excitons has attracted considerable interest in purely organic luminescent materials at room temperature[17-27]. One strategy to realize room temperature phosphorescence (RTP) is promoting intersystem crossing (ISC) through precise molecular design with heavy halogen atoms, aromatic carbonyl, *etc*. Notably, the rate constant of ISC (k_{isc}) is proportional to the eighth power of atomic number[28] ($k_{isc} \propto Z^8$, Equation S2), which means the heavy atoms can efficiently populate the triplet excitons. And the other is suppressing the non-radiative dissipation *via* the construction of a rigid environment utilizing crystal engineering, host-guest doping, polymerization and so forth[29-31]. Therefore, we rationally speculate that the modulation of the heavy halogen atoms enables purely organic phosphors with highly efficient luminescence under X-ray irradiation, since the halogen atoms not only promote the absorption of X-ray photons, but also make the triplet excitons bright for boosting luminescence because of SOC enhancement (Fig. 1a).

To validate our hypothesis, we designed and synthesized different organic material systems containing heavy halogen atoms (Fig. 1b). In addition, oxygen and nitrogen atoms are incorporated to favour n-π* transition, facilitating the ISC process on the basis of El-Sayed rule[32]. As a proof of concept, we firstly synthesized three isomers of 9,9'-(6-iodophenoxy-1,3,5-triazine-2,4-diyl)bis(9H-carbazole) (*o*-ITC, *m*-ITC, and *p*-ITC) with iodine atom modification. The chemical structures and their purities were systematically characterized by ^{1}H and ^{13}C NMR spectroscopies, single-crystal X-ray diffraction, elemental analysis, and high-performance liquid chromatography (Supplementary Section I, Supplementary Fig. 1). Under the radiation of UV lamp, strong luminescence was detected (Fig. 2a inset, Supplementary Fig. 2). After removing the UV lamp, the emission with a persistent time of several seconds was observed by naked eye (Fig. 2a inset). Within expectation, intense X-ray excited luminescence of these phosphors were achieved as well (insets in Fig. 2b).

[1]Frontiers Science Center for Flexible Electronics, Xi'an Institute of Flexible Electronics (IFE) and Xi'an Institute of Biomedical Materials & Engineering (IBME), Northwestern Polytechnical University, Xi'an, China. [2]Key Laboratory of Flexible Electronics (KLOFE) & Institute of Advanced Materials (IAM), Nanjing Tech University, Nanjing, China. [3]MOE Key Laboratory for Analytical Science of Food Safety and Biology, State Key Laboratory of Photocatalysis on Energy and Environment, College of Chemistry, Fuzhou University, Fuzhou, China. [4]SZU-NUS Collaborative Innovation Center for Optoelectronic Science and Technology, Shenzhen University, Shenzhen, China. [5]State Key Laboratory of Modern Optical Instrumentation, College of Optical Science and Engineering, Zhejiang University, Hangzhou, Zhejiang, China. [6]Hefei National Laboratory for Physical Sciences at the Microscale, University of Science and Technology of China, Hefei, China. [7]Department of Chemistry, National University of Singapore, Singapore, Singapore. [8]These authors contributed equally to this work. *e-mail: iamzfan@njtech.edu.cn; chmlx@nus.edu.sg; iamwhuang@njtech.edu.cn

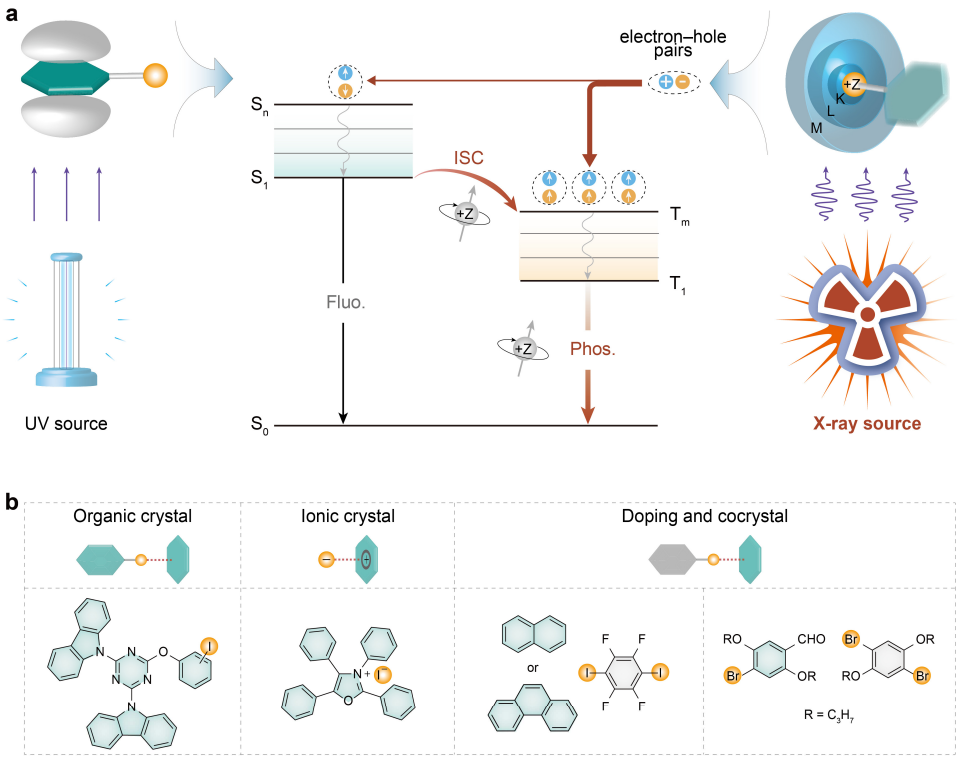

Fig. 1 | Schematic representation of the X-ray excited luminescence in purely organic materials. a, Typical mechanism of UV excited luminescence and proposed X-ray irradiated luminescence. Electrons located on frontier molecular orbital are excited by UV source to generate singlet Frenkel excitons, representing the UV light absorption process. After the aforementioned process, the molecules in excited state (S_n) rapidly relax to the lowest vibrational level of S_1, which subsequently return to ground state (S_0), accompanying by fluorescence. Molecules in the S_1 state can also undergo ISC process to the triplet states (T_m), following by internal conversion (IC) to lowest triplet state (T_1). However, the spin-forbidden origin of T_1 leads to a relatively weak phosphorescence. For X-ray excited luminescence processes, massive electrons and holes were firstly produced after X-ray source excites the inner electrons of heavy atoms. The next charge recombination process produces a larger ratio of triplet excitons according to spin statistics, harvesting the population of triplet excitons to generate dominated phosphorescence. **b,** Rational design of purely organic phosphors for X-ray excited luminescence. The heavy atoms such as Br and I are introduced to promote the absorption of X-ray and the ISC process in the meantime. The aromatic groups are designed to tune the RTP properties. Types of phosphors are involved in crystalline state, including organic crystal, organic ionic crystal, cocrystal and host-guest doping system.

Subsequently, we investigated the photoluminescence (PL) of the isomer phosphors in solid state under ambient conditions. As shown in Fig. 2a, three isomers all showed dual emission bands with one peak at around 390 nm and another highly resolved vibrionic emission peaks ranging from 500 to 700 nm. The latter emission band features long luminescence lifetimes of 46.49 ms for *o*-ITC (535 nm), 72.18 ms for *m*-ITC (525 nm), and 106.34 ms for *p*-ITC (530 nm), respectively (Fig. 2c, Supplementary Table 1), indicating the phosphorescence nature of the emission. It is noted that the vibrational emission peaks located between 500 and 700 nm are separated by approximately 1400 cm^{-1}, signifying that the lowest excited triplet states are π-localized excited states. Additionally, the maximum phosphorescence efficiencies of the *o*-ITC, *m*-ITC, and *p*-ITC phosphors reach up to 38.2%, 37.1%, and 19.1%, respectively (Supplementary Table 2).

In a further set of experiments, we explored the relatively X-ray excited emission properties of the isomers in solid state. From Fig. 2b, we found that the main bands of radioluminescence (RL) spectra were 535, 525, 530 nm for *o*-ITC, *m*-ITC and *p*-ITC, respectively. Especially, compared with the PL spectra, their corresponding RL spectra display the same emission wavelengths but remarkably dominant phosphorescence (Fig. 2b). The phosphorescence nature of the latter emission peaks was also illustrated through RL decay profiles (Supplementary Fig. 3). It is worthy to note that the integral area ratios of phosphorescence to fluorescence derived from RL (13.59, 11.76, and 6.55 for *o*-ITC, *m*-ITC, and *p*-ITC, respectively) are significantly larger than that of UV excited counterparts (1.32, 0.81, and 0.48 for *o*-ITC, *m*-ITC, and *p*-ITC, respectively) (Fig. 2d). This finding indicates the existence of different photophysical mechanisms between PL and RL processes.

We then selected *o*-ITC as a model to investigate the radiostability of the organic phosphors. Importantly, when the phosphor was exposed to high dose rate of X-ray (278 μGy/s) for continuous 30 minutes, the RL intensity still remained around 94% of the initial value. Moreover, the RL intensity recovered completely after keeping away from the exposure of X-rays for one hour. This process

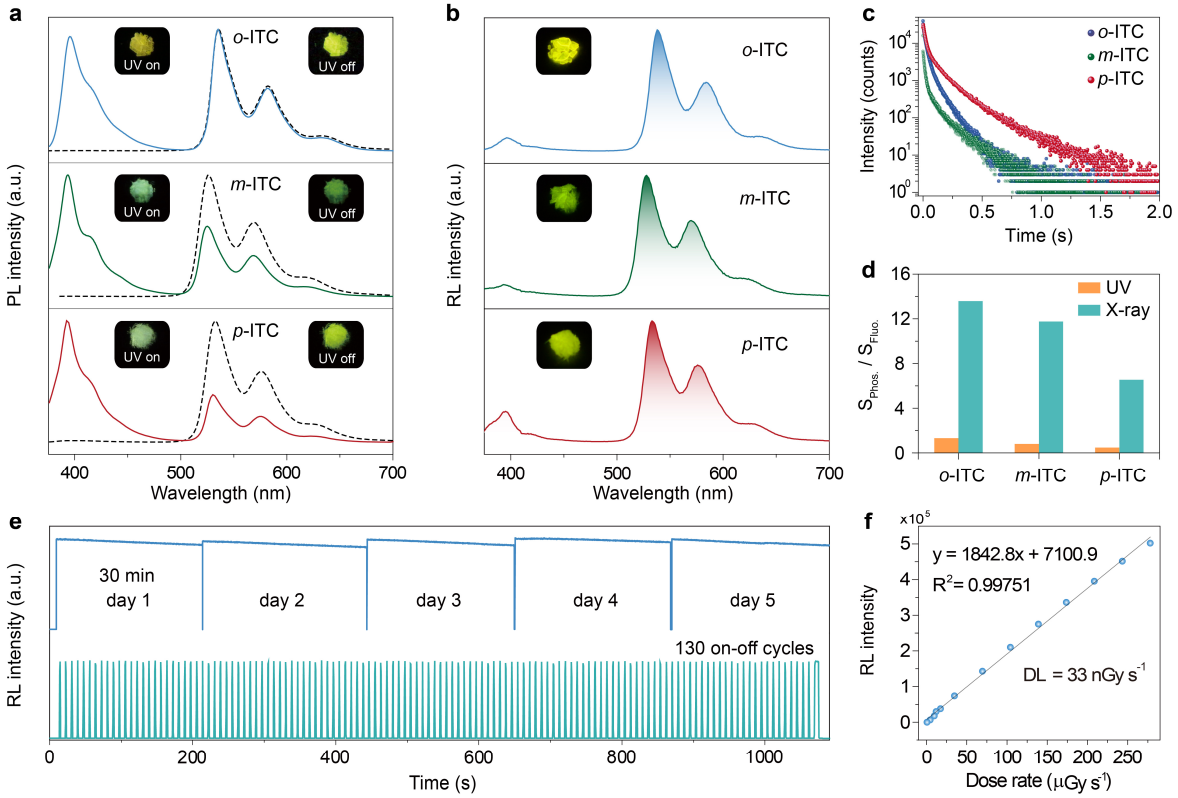

Fig. 2 | Photoluminescence and X-ray excited luminescence characterization of iodine containing isomers in crystalline state under ambient conditions. **a,** Steady-state photoluminescence (PL, solid lines) and room temperature phosphorescence (dashed lines) spectra of *o*-ITC, *m*-ITC, and *p*-ITC, respectively. The left insets show the photographs of steady-state luminescence with the excitation of a 365 nm UV lamp, and the right ones display the photographs of RTP after removing the UV source. **b**, Radioluminescence (RL) spectra of the three isomers by X-ray with a dose rate of 278 μGy/s. Insets indicate the X-ray excited photographs of the three isomers. **c**, Lifetime profiles of emission bands around 530 nm of the isomers under the excitation at 365 nm. **d**, Ratios of $S_{Phos.}/S_{Fluo.}$under the excitation of UV and X-ray, where $S_{Phos.}$ and $S_{Fluo.}$ represent the integral area of phosphorescence and fluorescence region, respectively. **e**, Radiostability of emission at 535 nm for the *o*-ITC phosphor against continuous irradiation (top) and repeated on-off cycles of X-ray irradiation (bottom) under the dose rate of 278 μGy/s. **f**, Dose rate dependence of the RL intensity of *o*-ITC in a range of 0.688 to 278 μGy/s. The detection limit (DL) is calculated on the 3σ/slope method.

is reversible (Fig. 2e). Moreover, its intensity kept stable even under the X-ray excitation with repeated 130 on-off circles (Fig. 2e). Apart from the influence of irradiation time on radiostability, the detection limit of X-ray dosage is also critical for practical applications. As shown in Fig. 2f, the X-ray excited luminescence intensity values were exceptionally found to be linearly correlated with the dose rate of X-ray, indicating the detection limit of 33 nGy/s. It is about 167 times lower than the classical dosage for X-ray diagnostics (5.5 μGy/s) [33].

To deeply gain an insight into the mechanism of X-ray excited purely organic luminescence, we designed and synthesized a series of control molecules based on *o*-ITC through varying the iodine atom to bromine, chlorine, and hydrogen, which are named as *o*-BrTC, *o*-ClTC, and *o*-HTC, respectively (Supplementary Scheme 1). We compared the absorption coefficient of the four molecules (*o*-ITC, Z_{max} = 53, $K_α$ = 33. 2 keV; *o*-BrTC, Z_{max} = 35, $K_α$ = 13.5 keV; *o*-ClTC, Z_{max} = 17, $K_α$ = 2.82 keV; *o*-HTC, Z_{max} = 6, $K_α$ = 0.285 keV. Fig. 3a). It is obvious that heavy atoms play an important role in absorbing X-ray photons. Apart from resonant absorption edges, the absorption coefficient of *o*-ITC across the entire energy region (1-1000 keV) is higher than that of *o*-BrTC, *o*-ClTC, and *o*-HTC (Fig. 3a). Equally importantly, the aforementioned tendency matches well with the relative phosphorescence proportion, namely, there is a positive correlation between phosphorescence proportion and heavy atom number (Fig. 3b). Furthermore, we explored the electron escaping process of *o*-ITC *via* X-ray photoelectron spectroscopic (XPS, Supplementary Fig. 4). We can clearly figure out that the electrons of 3*d* of iodine, 1*s* of oxygen, 1*s* of nitrogen, and 1*s* of carbon atom are mainly escaped when excited by soft X-rays. The generation of electrons and holes upon X-ray irradiation in the above-mentioned process can be proved using the photoconductive gain experiment shown in Fig. 3c.[35]

From the single crystal analysis of *o*-ITC, each molecule is confined by neighboring molecules with multiple intermolecular interactions with distances of 2.615 (C-H···O), 2.886 (C-H···π), 3.303 (π···π), and 3.481 Å (C-I···π) (Fig. 3d, Supplementary Fig. 5), forming a rigid surrounding to effectively suppress the non-radiative decay of triplet excitons. Significantly, the iodine atom has such a

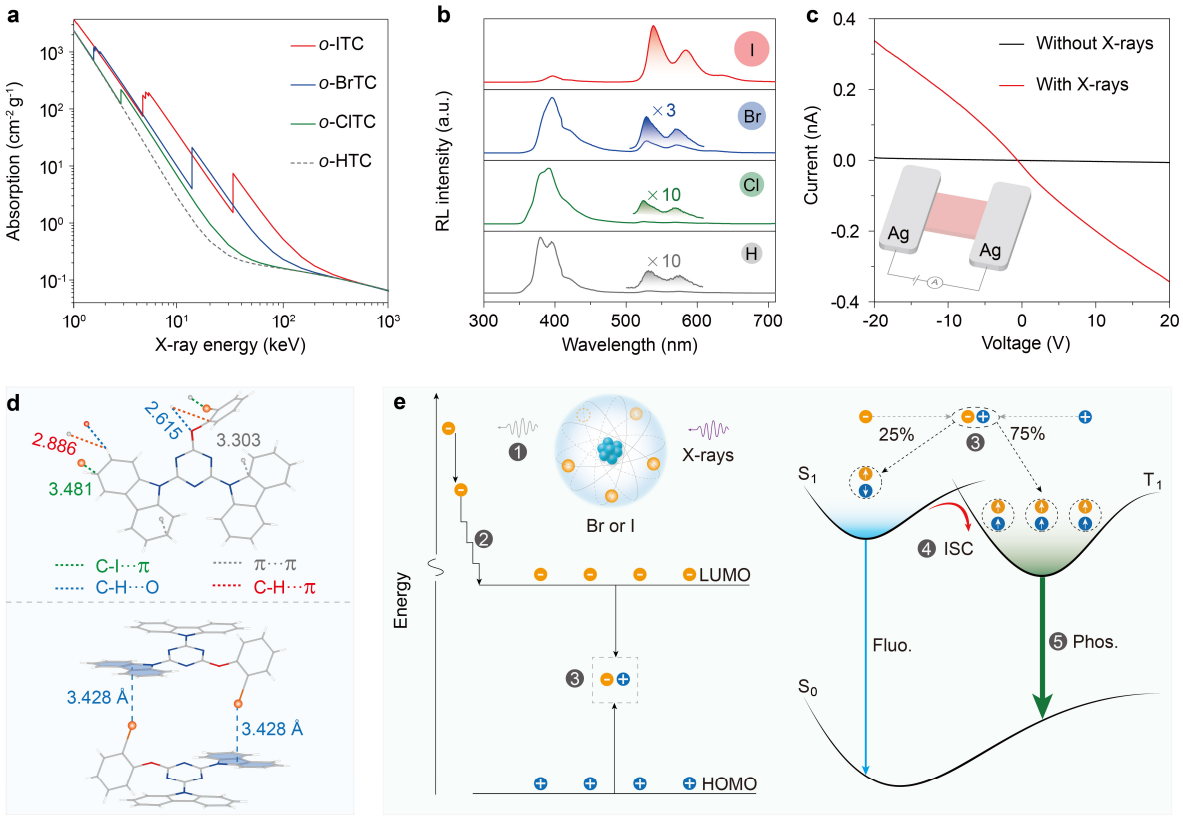

Fig. 3 | Proposed mechanism of X-ray excited luminescence in purely organic phosphors at room temperature. a, Measured X-ray absorption spectra of *o*-ITC, *o*-BrTC, *o*-ClTC, and *o*-HTC. The attenuation coefficient μ were obtained in photon cross-section database[34]. **b**, The RL spectra of *o*-ITC, *o*-BrTC, *o*-ClTC, and *o*-HTC phosphors at the dose rate of 278 μGy/s. To be seen clearly, the phosphorescent bands are multiplied by suitable times. **c**, Current-voltage curves of the constructed photodetector measured in the dark and under X-ray illumination (dose rate: 2.094 mGy/s). Inset: schematic showing the construction of the photodetector. Silver (Ag) electrodes are deposited onto the crystal of *o*-ITC for hole-electron extraction. The distance between two Ag electrodes is 3 mm. **d**, Molecular arrangement of the *o*-ITC molecules in single crystal. Noted that four types of intermolecular interactions between neighboring molecules are shown in different colours. **e**, Plausible energy transfer processes for RL in purely organic phosphors. Upon the excitation of X-ray, electrons (orange circle) are ejected mainly from the inner shell of heavy atoms, generating high energy holes (blue circle) in core levels (Step 1). Subsequently, the high energy electrons interact with the outer shells of atoms, resulting in an avalanche of secondary carriers. This process continues until the generated electrons and holes can never create further ionization, leading to the thermalization in LUMO and HOMO (Step 2). Then the recombination of electrons and holes produces excitons in a ratio of 25% singlet excitons to 75% triplet excitons (Step 3). Because of the strong SOC effect, the ISC process is enhanced (Step 4), generating a relatively dominant phosphorescent emission in comparison with UV-excited photoluminescence (Step 5).

short distance with carbazole plane (3.428 Å) that the ISC process concerning S_1 to T_n and T_1 to S_0 is enhanced, generating efficient RTP. To probe this mechanism, we performed first-principle time-dependent density functional theory (TD-DFT, Supplementary Fig. 6), SOC constants (ξ) of S_1 to T_n of *o*-ITC (S_1-T_2, 2.79 cm^{-1}) is much larger than that (S_1-T_3, 0.69 cm^{-1}) of *o*-HTC without heavy atom effect. Furthermore, the rate constants for ISC (k_{isc}) and phosphorescence (k_p) indicate improved values after halogenation (Supplementary Table 3). Specially, k_p for *o*-ITC is 11.6 s^{-1}, which is 120 times higher than that of *o*-HTC (0.097 s^{-1}). These results proved the enhanced ISC process with assistance of heavy atom, further taking advantage of bright triplet excitons to improve the RL properties of the organic phosphors.

Taking these results together, we proposed a plausible mechanism for RL in purely organic phosphors (Fig. 3e). Three stages are involved during the X-ray excited luminescence process. At the first conversion stage, X-ray photons are mainly absorbed, primarily through photoelectric effect, by heavy atoms in molecules. X-ray photons possess high enough energy (5–50 keV in this work) to "kick out" inner electrons, generating electrons and holes with high-energy. Subsequently, the fast photoelectrons further give rise to a large amount of secondary electrons. Undergoing a repeated process, the high energy electrons and holes are rapidly thermalized in the lowest unoccupied molecular orbital (LUMO) and the highest occupied molecular orbital (HOMO) of the phosphors, respectively. Then the electrons and holes recombined to produce massive singlet and

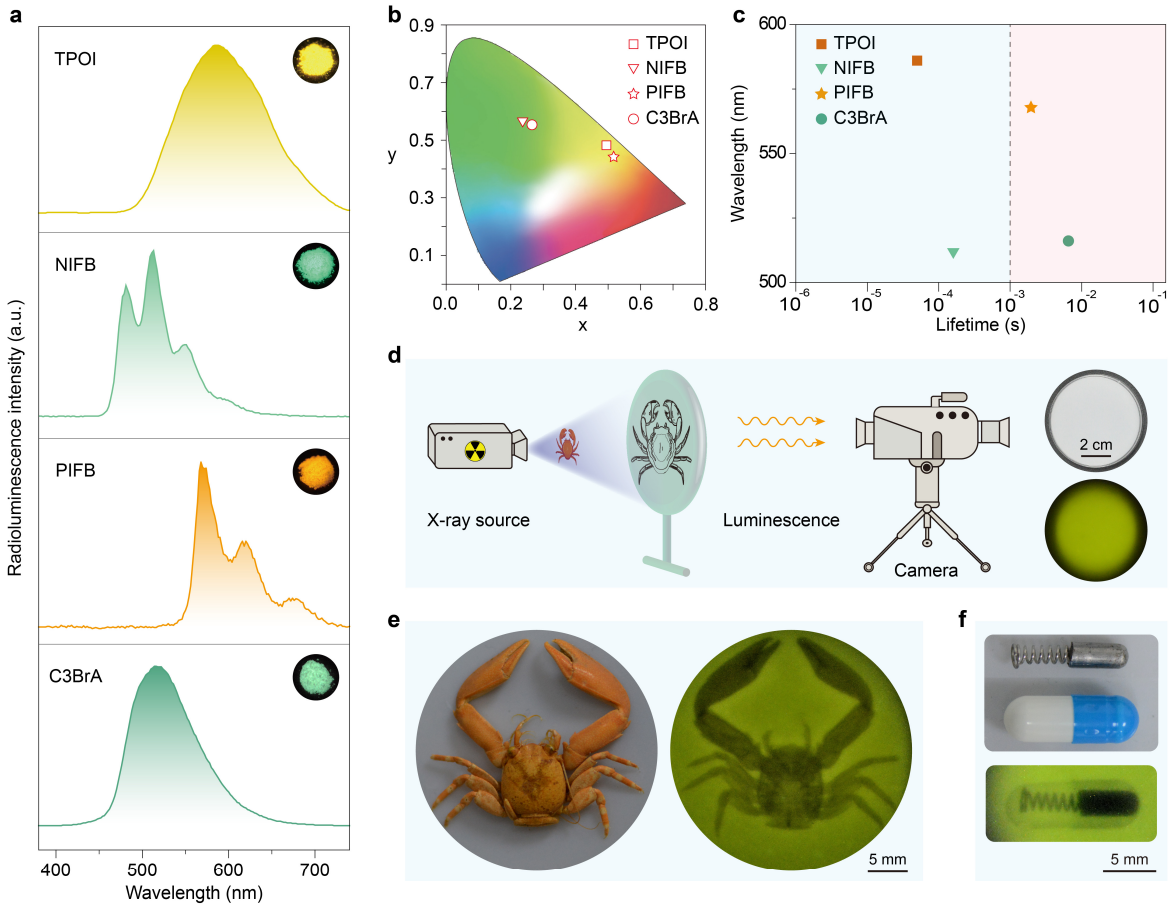

Fig. 4 | Versatile pure organic phosphors for X-ray excited luminescence and primary demonstration for the radiography application under ambient conditions. a, The RL spectra and radioluminescent photographs of ionic crystal (TPOI), cocrystal (NIFB and PIFB), and doping system (C3BrA) at the dose rate of 278 μGy/s. **b**, CIE chromaticity coordinate diagram of RL for the organic phosphors. **c**, The plot of maximum emission wavelengths and average lifetimes of the phosphors. The lifetimes have a wide range from microseconds to sub-seconds. **d**, Schematic of the radiography system. A PDMS film (diameter: 6 cm) containing *o*-ITC was used as background luminescent material, and a specimen of crab was placed between X-ray source and digital camera. **e**, Bright-field (left) and dark-field photographs under exposure of X-ray (right) of the crab. **f**, Bright-field (up) and dark-field photographs under exposure of X-ray (bottom) of the non-transparent capsule with metallic spring and cylinder.

triplet excitons with a 1:3 ratio according to spin statistics. The radiative decay processes of the singlet and triplet excitons generate fluorescence and phosphorescence, respectively. Notably, the bright triplet excitons aroused by strong SOC effect endow purely organic phosphors with efficient phosphorescent RL, compared with PL by UV-light irradiation. The proportion of the generated singlet excitons for *o*-ITC was calculated to be 22% at maximum upon X-ray irradiation (Supplementary Section II), which fits well with theoretical value. Considering the proposed mechanism, we explored the luminescent properties of molecules, *o*-BrTC, *o*-ClTC, and *o*-HTC, under excitation of UV and X-ray. As a result, X-ray excited spectra indeed displayed larger phosphorescence proportion (Supplementary Fig. 7).

To verify the universality of our principle to achieve X-ray excited purely organic phosphors, we further synthesized a succession of heavy-atom-containing materials such as organic ionic crystal (TPOI), cocrystals (NIFB and PIFB), and doping crystal (C3BrA) (Fig. 4a, Supplementary Scheme 1). As expected, these organic materials all show intense X-ray excited luminescence, and the different chromophores exhibit distinguishing emission colours. Specially, TPOI showed RL at 586 nm, NIFB and PIFB displayed RL with maximum emission peak at 513 nm and 568 nm, respectively. For the doping material C3BrA, the RL peak was located at 516 nm. As can be seen, these materials display various emission colours in the visible region (Fig. 4b) and lifetimes with different orders of magnitudes (Fig. 4c, Supplementary Fig. 9). The aforementioned varieties of material systems, emission colours, and lifetimes validate the generalizability of our strategy, demonstrating potential applications in various fields with different requirements.

Regarding of the intense X-ray excited luminescence, we applied the *o*-ITC phosphor to X-ray radiography. We fabricated a flexible polydimethylsiloxane (PDMS) film of *o*-ITC as the background

substrate (Supplementary Fig. 10), which showed the same RL profile as bulk crystal. Then a sample was placed between X-ray source and *o*-ITC film (Fig. 4d). Owing to the relatively higher absorption of X-ray photons, the hard shell of the crab can be visualized directly using a commercial digital camera (Fig. 4e). The application of direct X-ray contrast imaging of organism also shows the possibility to inspect the inner structure of materials that opaque to visible light. We set a further inspection of non-transparent capsule with built-in metallic spring and cylinder. Using the same method, we can also figure out the pattern of metallic material. (Fig. 4f). We can reasonably infer that X-ray photons can easily penetrate through the areas without metal to excite the *o*-ITC material, so that the RL will apparently tell the boundary of metallic spring and cylinder. These results demonstrate the potential of X-ray excited purely organic phosphors for the radiography applications.

In conclusion, we have developed a design principle to obtain X-ray excited purely organic phosphors. The modulation of heavy halogen atoms can cooperatively promote the absorption of X-ray photons and the ISC process, leading to intense X-ray excited luminescence of the phosphors under ambient conditions. By varying the material species from small molecular crystals, ionic crystals to host-guest doping system and cocrystals, the X-ray excited intense luminescence with diverse emission colours and lifetimes can be achieved as well, indicating the universality of our principle. Utilizing the RL property, we made real of the radio contrast imaging both in the biological organism and the industrial product. Importantly, this finding not only provides a fundamental design principle for realizing efficient X-ray excited luminescence in purely organic materials, but also extends the application scope of the organic phosphorescent materials to optoelectronics and biomedicine.

References

1. Büchele, P. *et al.* X-ray imaging with scintillator-sensitized hybrid organic photodetectors. *Nat. Photonics.* **9**, 843-848 (2015).
2. Chen, Q. *et al.* All-inorganic perovskite nanocrystal scintillators. *Nature* **561**, 88-93 (2018).
3. Fan, W. *et al.* Breaking the depth dependence by nanotechnology-enhanced X-ray-excited deep cancer theranostics. *Adv. Mater.* **31**, 1806381 (2019).
4. Gandini, M. *et al.* Efficient, fast and reabsorption-free perovskite nanocrystal-based sensitized plastic scintillators. *Nat. Nanotechnol.* **15**, 462-468 (2020).
5. Weber, M. J. Inorganic scintillators: today and tomorrow. *J. Lumin.* **100**, 35-45 (2002).
6. Kim, Y. C. *et al.* Printable organometallic perovskite enables large-area, low-dose X-ray imaging. *Nature* **550**, 87-91 (2017).
7. Shrestha, S. *et al.* High-performance direct conversion X-ray detectors based on sintered hybrid lead triiodide perovskite wafers. *Nat. Photonics.* **11**, 436-440 (2017).
8. Pan, W. *et al.* $Cs_2AgBiBr_6$ single-crystal X-ray detectors with a low detection limit, *Nat. Photonics.* **11**, 726-732 (2017).
9. Lu, K. *et al.* Low-dose X-ray radiotherapy–radiodynamic therapy via nanoscale metal–organic frameworks enhances checkpoint blockade immunotherapy. *Nat. Biomed. Eng.* **2**, 600-610 (2018).
10. Nikl, M. & Yoshikawa, A. Recent R&D trends in inorganic single-crystal scintillator materials for radiation detection. *Adv. Optical Mater.* **3**, 463-481 (2015).
11. Lusic, H. & Grinstaff, M. W. X-ray-computed tomography contrast agents. *Chem. Rev.* **113**, 1641-1666. (2012).
12. Hajagos, T., Liu, C., Cherepy, N. & Pei, Q. High-Z sensitized plastic scintillators: a review. *Adv. Mater.* **30**, 1706956-1706968 (2018).
13. Chen, X., Song, J., Chen, X. & Yang, H. X-ray-activated nanosystems for theranostic applications. *Chem. Soc. Rev.* **48**, 3073-3101 (2019).
14. Baldo, M. A., Thompson, M. E. & Forrest, S. R. High-efficiency fluorescent organic light-emitting devices using a phosphorescent sensitizer. *Nature* **403**, 750-753 (2000).
15. Rao, A. *et al.* The role of spin in the kinetic control of recombination in organic photovoltaics. *Nature* **500**, 435-439 (2013).
16. Thompson, N. J. *et al.* Energy harvesting of non-emissive triplet excitons in tetracene by emissive PbS nanocrystals. *Nat. Mater.* **13**, 1039-1043 (2014).
17. Zhang, G., Palmer, G., Dewhirst, M. & Fraser, C. A dual-emissive-materials design concept enables tumour hypoxia imaging. *Nat. Mater.* **8**, 747-751 (2009).
18. Yuan, W. *et al.* Crystallization-induced phosphorescence of pure organic luminogens at room temperature. *J. Phys. Chem. C* **114**, 6090-6099 (2010).
19. An, Z. *et al.* Stabilizing triplet excited states for ultralong organic phosphorescence. *Nat. Mater.* **14**, 685-690 (2015).
20. Yang, Z. *et al.* Intermolecular electronic coupling of organic units for efficient persistent room-temperature phosphorescence. *Angew. Chem. Int. Ed.* **55**, 2181-2185 (2016).
21. Lucenti, E. *et al.* Cyclic triimidazole derivatives: intriguing examples of multiple emissions and ultralong phosphorescence at room temperature. *Angew. Chem. Int. Ed.* **56**, 16302-16307 (2017).
22. Xie, Y. *et al.* How the molecular packing affects the room temperature phosphorescence in pure organic compounds: ingenious molecular design, detailed crystal analysis, and rational theoretical calculations. *Adv. Mater.* **29**, 1606829 (2017).
23. Wang, J. *et al.* A facile strategy for realizing room temperature phosphorescence and single molecule white light emission. *Nat. Commun.* **9**, 2963 (2018).
24. Su, Y. *et al.* Ultralong room temperature phosphorescence from amorphous organic materials toward confidential information encryption and decryption. *Sci. Adv.* **4**, 9732-9744 (2018).
25. Salla, C. A. *et al.* Persistent solid-state phosphorescence and delayed fluorescence at room temperature by a twisted hydrocarbon. *Angew. Chem. Int. Ed.* **58**, 6982-6986 (2019).
26. Ma, H., Peng, Q., An, Z., Huang, W. & Shuai, Z. Efficient and long-lived room-temperature organic phosphorescence: theoretical descriptors for molecular designs. *J. Am. Chem. Soc.* **141**, 1010-1015 (2019).
27. Li, W. *et al.* Selective expression of chromophores in a single molecule: soft organic crystals exhibiting full−colour tunability and dynamic triplet−exciton behaviours. *Angew. Chem. Int. Ed.* **59**, 3739-3745 (2020).
28. Baryshnikov, G., Minaev, B. & Ågren, H. Theory and calculation of the phosphorescence phenomenon. *Chem. Rev.* **117**, 6500-6537 (2017).

29. Bolton, O., Lee, K., Kim, H., Lin, K. & Kim, J. Activating efficient phosphorescence from purely organic materials by crystal design. *Nat. Chem.* **3**, 205-210 (2011).
30. Gu, L. *et al.* Colour-tunable ultra-long organic phosphorescence of a single-component molecular crystal. *Nat. Photonics.* **13**, 406-411 (2019).
31. Zhang, T. *et al.* Molecular engineering for metal-free amorphous materials with room-temperature phosphorescence. *Angew. Chem. Int. Ed.* **59**, 11206-11216 (2020).
32. El-Sayed, M. A. Triplet state: its radiative and nonradiative properties. *Acc. Chem. Res.* **1**, 8-16 (1968).
33. Wei, H. *et al.* Sensitive X-ray detectors made of methylammonium lead tribromide perovskite single crystals. *Nat. Photonics.* **10**, 333-339 (2016).
34. Berger, M. J. *et al. XCOM: photon cross sections database*; https://www.nist.gov/pml/xcom-photon-cross-sections-database (2013).
35. Zhuang, R. *et al.* Highly sensitive X-ray detector made of layered perovskite-like $(NH_4)_3Bi_2I_9$ single crystal with anisotropic response. *Nat. Photonics.* **13**, 602-608 (2019).

Acknowledgements
This work is supported by the National Natural Science Foundation of China (21975120, 21875104, 91833304, 21973043, 51673095 and 61935017), the Natural Science Foundation of Jiangsu Province (BK20150962), Postdoctoral Innovative Talents Support Program (BX20200278), Projects of International Cooperation and Exchanges NSFC (51811530018) and the Fundamental Research Funds for the Central Universities.

Author contributions
X.W., H.S., Z.A., X.L and W.H. conceived the experiments. X.W., Z.A., X.L. and W.H. prepared the paper. X.W., H.S., W.Y., L.S., X.Y., G.Y, Z.Z., M.S., C.L., J.Z., and C.D. were primarily responsible for the experiments. J.Z., X.O., Y.T., Q.C., Y.W., and H.Y. were responsible for X-ray related experiments. H.W., Q.W., and W.J. performed lifetime and quantum yield measurements. H.M. and X.J contributed to TD-DFT calculations. X.X., J.W., and G.Z. gave suggestions of the manuscript. All authors contributed to the data analyses.

Additional information
Supplementary information is available in the online version of the paper. Reprints and permissions information is available online at www.nature.com/reprints. Correspondence and requests for materials should be addressed to Z.A., X.L. or W.H.

Competing financial interests
The authors declare no competing financial interests.

Figures

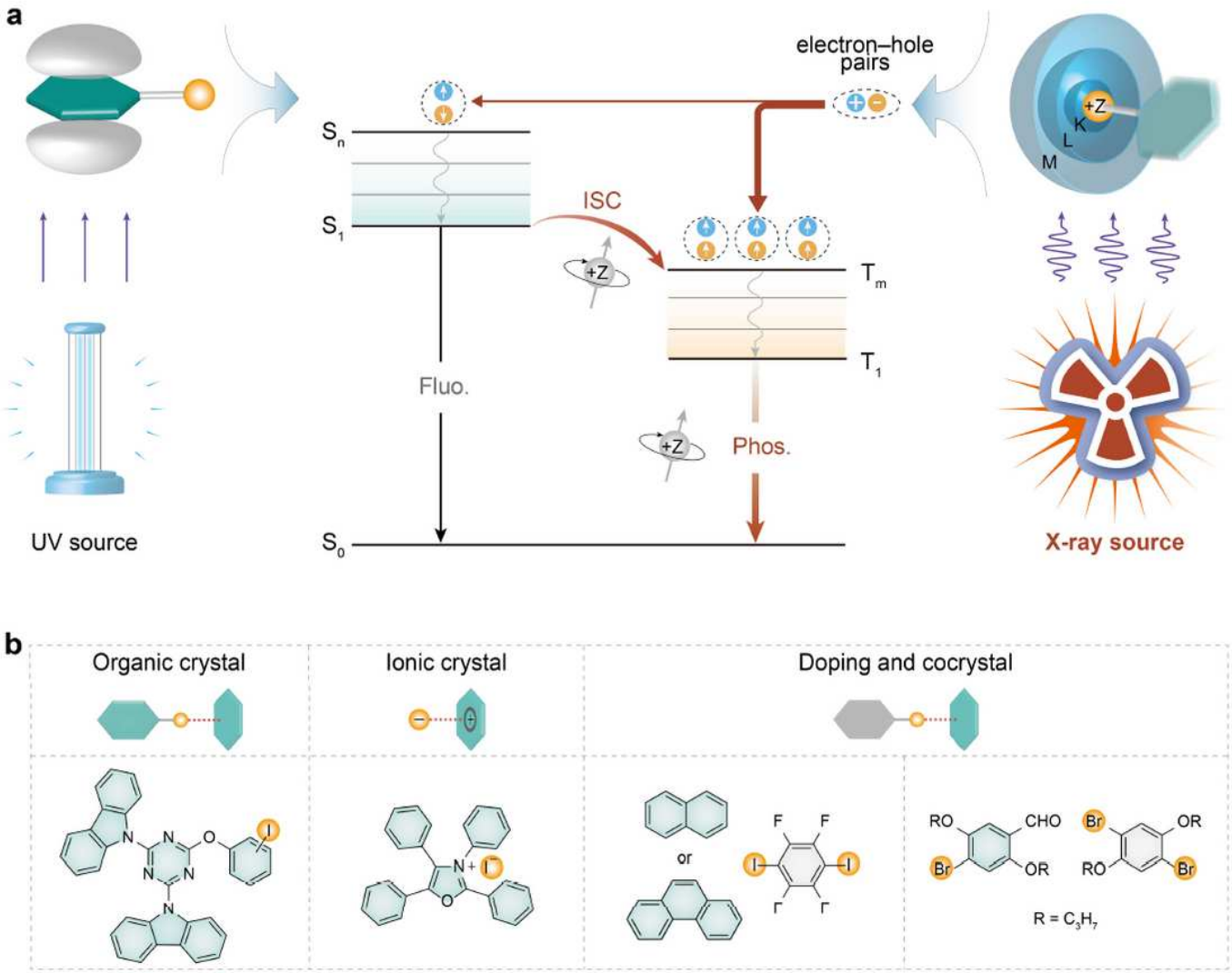

Figure 1

Schematic representation of the X‐ray excited luminescence in purely organic materials. a, Typical mechanism of UV excited luminescence and proposed X‐ray irradiated luminescence. Electrons located on frontier molecular orbital are excited by UV source to generate singlet Frenkel excitons, representing the UV light absorption process. After the aforementioned process, the molecules in excited state (Sn) rapidly relax to the lowest vibrational level of S1, which subsequently return to ground state (S0), accompanying by fluorescence. Molecules in the S1 state can also undergo ISC process to the triplet states (Tm), following by internal conversion (IC) to lowest triplet state (T1). However, the spin‐forbidden origin of T1 leads to a relatively weak phosphorescence. For X‐ray excited luminescence processes, massive electrons and holes were firstly produced after X‐ray source excites the inner electrons of heavy atoms. The next charge recombination process produces a larger ratio of triplet excitons according to spin statistics, harvesting the population of triplet excitons to generate dominated phosphorescence. b, Rational design of purely organic phosphors for X‐ray excited luminescence. The heavy atoms such as Br

and I are introduced to promote the absorption of X‐ray and the ISC process in the meantime. The aromatic groups are designed to tune the RTP properties. Types of phosphors are involved in crystalline state, including organic crystal, organic ionic crystal, cocrystal and host‐guest doping system.

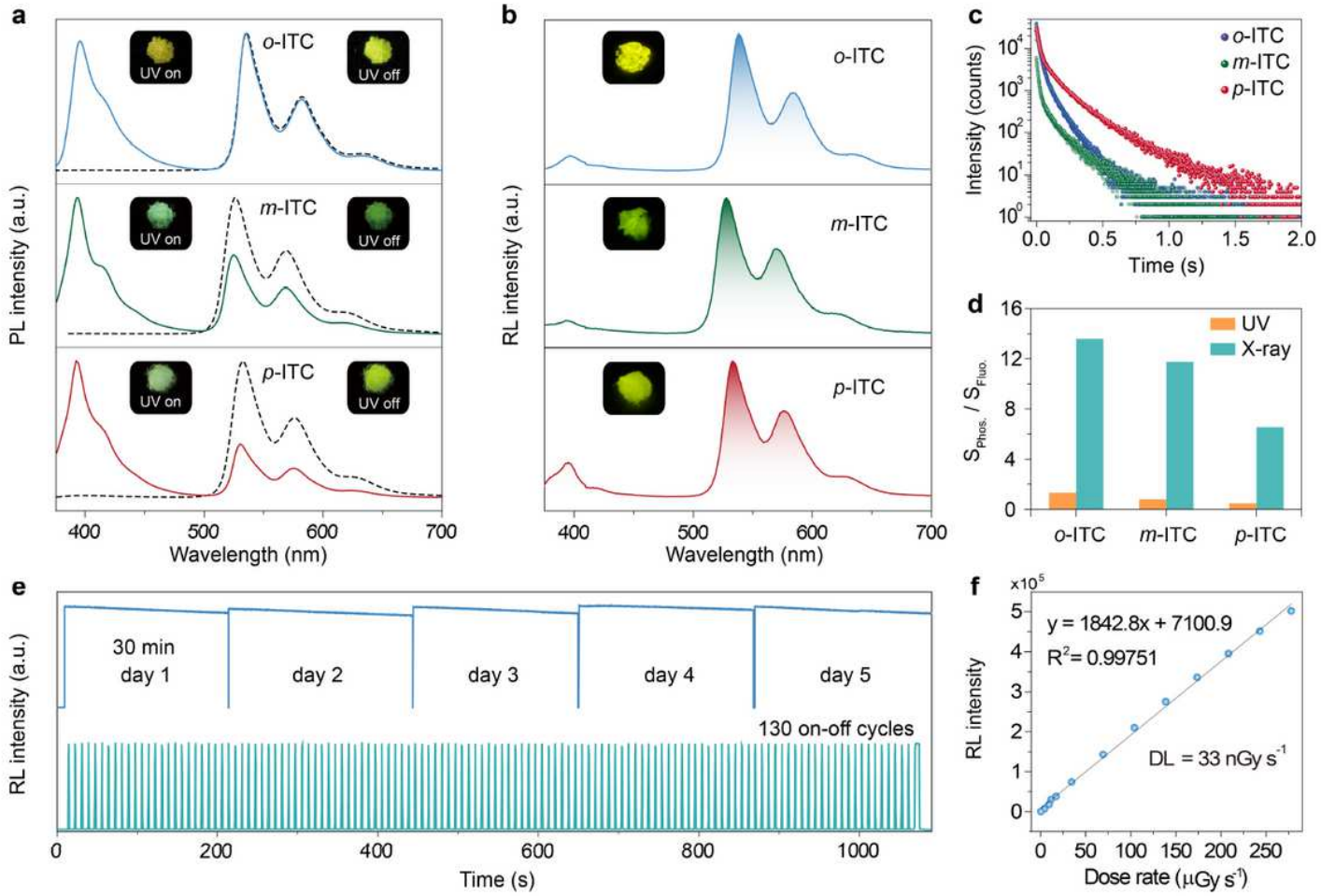

Figure 2

Photoluminescence and X‐ray excited luminescence characterization of iodine containing isomers in crystalline state under ambient conditions. a, Steady‐state photoluminescence (PL, solid lines) and room temperature phosphorescence (dashed lines) spectra of o‐ITC, m‐ITC, and p‐ITC, respectively. The left insets show the photographs of steady‐state luminescence with the excitation of a 365 nm UV lamp, and the right ones display the photographs of RTP after removing the UV source. b, Radioluminescence (RL) spectra of the three isomers by X‐ray with a dose rate of 278 μGy/s. Insets indicate the X‐ray excited photographs of the three isomers. c, Lifetime profiles of emission bands around 530 nm of the isomers under the excitation at 365 nm. d, Ratios of SPhos./SFluo.under the excitation of UV and X‐ray, where SPhos. and SFluo. represent the integral area of phosphorescence and fluorescence region, respectively. e, Radiostability of emission at 535 nm for the o‐ITC phosphor against continuous irradiation (top) and repeated on‐off cycles of X‐ray irradiation (bottom) under the dose rate of 278 μGy/s. f, Dose rate dependence of the RL intensity of o‐ITC in a range of 0.688 to 278 μGy/s. The detection limit (DL) is calculated on the 3σ/slope method.

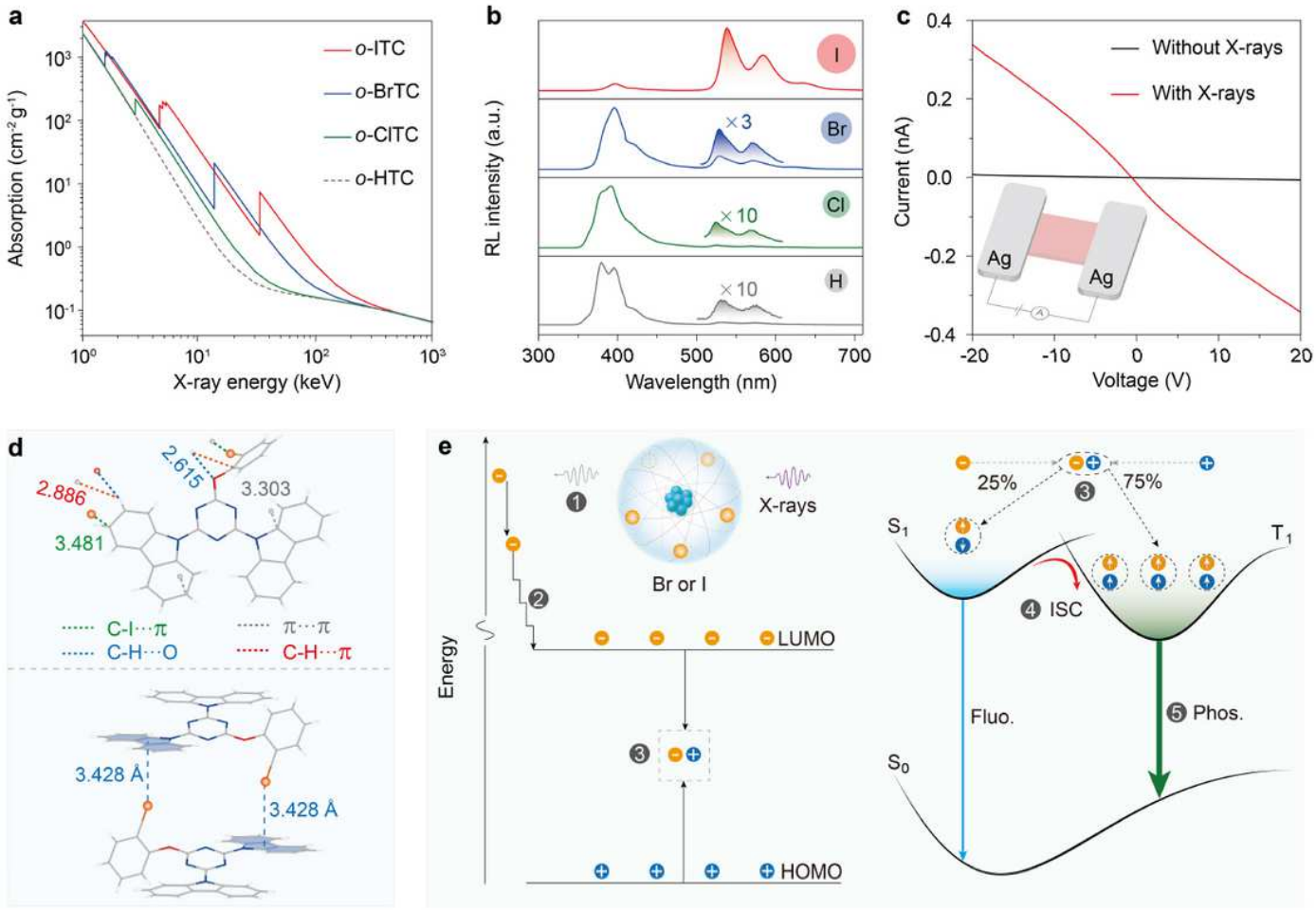

Figure 3

Proposed mechanism of X‐ray excited luminescence in purely organic phosphors at room temperature. a, Measured X‐ray absorption spectra of o‐ITC, o‐BrTC, o‐ClTC, and o‐HTC. The attenuation coefficient μ were obtained in photon cross‐section database34. b, The RL spectra of o‐ITC, o‐BrTC, o‐ClTC, and o‐HTC phosphors at the dose rate of 278 μGy/s. To be seen clearly, the phosphorescent bands are multiplied by suitable times. c, Currentvoltage curves of the constructed photodetector measured in the dark and under X‐ray illumination (dose rate: 2.094 mGy/s). Inset: schematic showing the construction of the photodetector. Silver (Ag) electrodes are deposited onto the crystal of o‐ITC for hole‐electron extraction. The distance between two Ag electrodes is 3 mm. d, Molecular arrangement of the o‐ITC molecules in single crystal. Noted that four types of intermolecular interactions between neighboring molecules are shown in different colours. e, Plausible energy transfer processes for RL in purely organic phosphors. Upon the excitation of X‐ray, electrons (orange circle) are ejected mainly from the inner shell of heavy atoms, generating high energy holes (blue circle) in core levels (Step 1). Subsequently, the high energy electrons interact with the outer shells of atoms, resulting in an avalanche of secondary carriers. This process continues until the generated electrons and holes can never create further ionization, leading to the thermalization in LUMO and HOMO (Step 2). Then the recombination of electrons and holes produces excitons in a ratio of 25% singlet excitons to 75% triplet excitons (Step 3). Because of the strong

SOC effect, the ISC process is enhanced (Step 4), generating a relatively dominant phosphorescent emission in comparison with UV‐excited photoluminescence (Step 5).

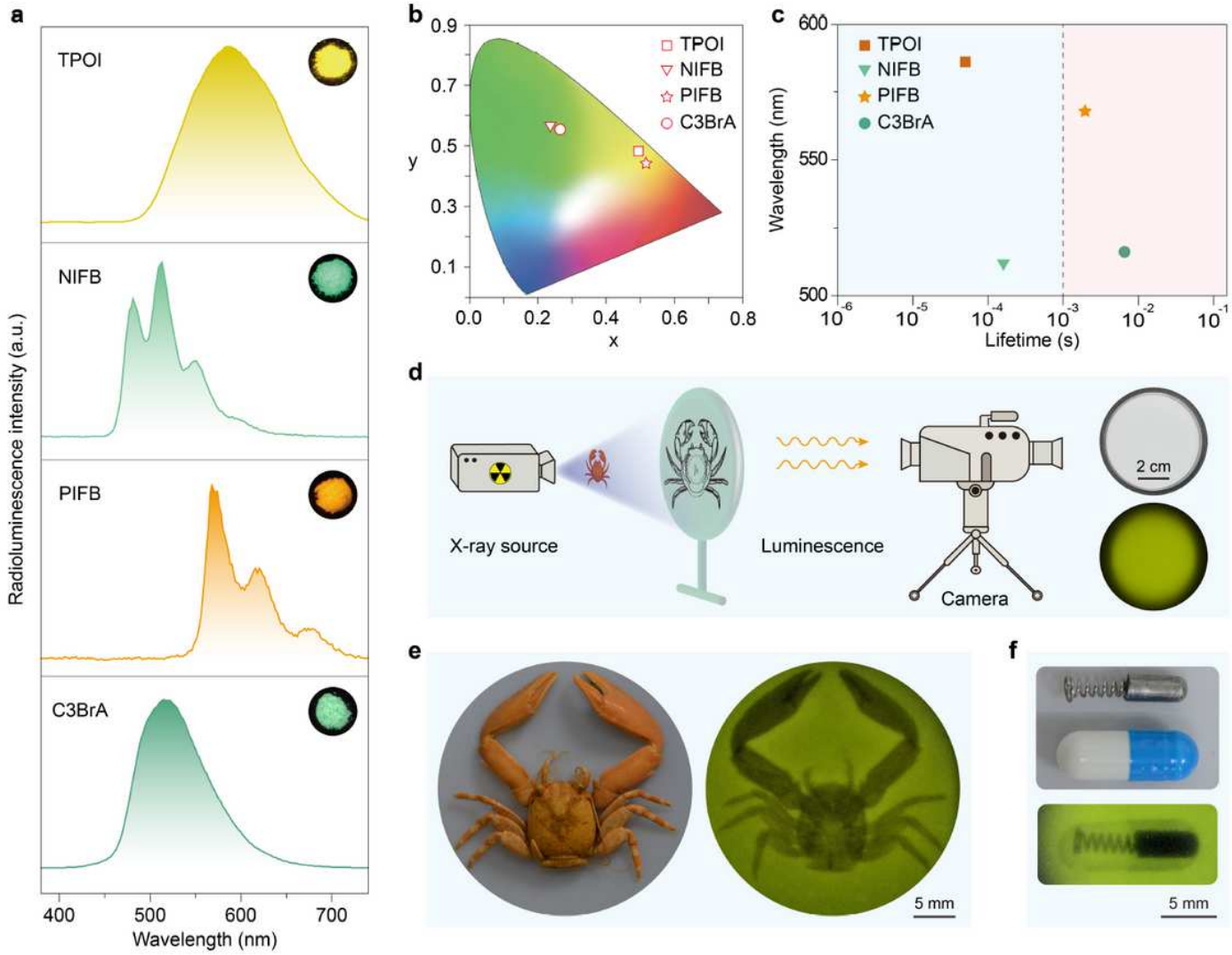

Figure 4

Versatile pure organic phosphors for X‐ray excited luminescence and primary demonstration for the radiography application under ambient conditions. a, The RL spectra and radioluminescent photographs of ionic crystal (TPOI), cocrystal (NIFB and PIFB), and doping system (C3BrA) at the dose rate of 278 μGy/s. b, CIE chromaticity coordinate diagram of RL for the organic phosphors. c, The plot of maximum emission wavelengths and average lifetimes of the phosphors. The lifetimes have a wide range from microseconds to sub‐seconds. d, Schematic of the radiography system. A PDMS film (diameter: 6 cm) containing o‐ITC was used as background luminescent material, and a specimen of crab was placed between X‐ray source and digital camera. e, Bright‐field (left) and dark‐field photographs under exposure of X‐ray (right) of the crab. f, Bright‐field (up) and dark‐field photographs under exposure of X‐ray (bottom) of the non‐transparent capsule with metallic spring and cylinder.

Supplementary Files

This is a list of supplementary files associated with this preprint. Click to download.

- SupplementaryInformation.pdf